

Limitations of accuracy in PIV due to individual variations of particle image intensities

Holger Nobach · Eberhard Bodenschatz

Received: 13 November 2007 / Revised: 19 January 2009 / Accepted: 30 January 2009 / Published online: 28 February 2009
© The Author(s) 2009. This article is published with open access at Springerlink.com

Abstract The effect of independent variations of the intensity of individual tracer particles between consecutive images on the accuracy of common displacement estimation methods in particle image velocimetry (PIV) is investigated. Such variations can be observed, e.g., in flows with components perpendicular to the illumination sheet, leading to out-of-plane displacements of the tracer particles. The achievable accuracy of PIV measurements is shown to be limited by this effect alone to be of the order of 0.1 pixel, yielding a basic limitation of the PIV technique.

1 Introduction

Particle image velocimetry (PIV) has become the prime choice for processing image-based flow measurements in fluid dynamics experiments. The basic algorithm of digital PIV processing (Utami et al. 1991; Willert and Gharib 1991; Keane and Adrian 1992; Westerweel 1993) utilizes the cross-correlation of image sub-spaces for local displacement estimation from two consecutively acquired images of a tracer-particle-laden flow.

A variety of image processing techniques using sub-pixel interpolations have been applied in the past to significantly improve the accuracy of the particle displacement measurement beyond the nominal resolution of the optical sensor. These include:

- Sub-pixel interpolation of the correlation planes, e.g. the peak centroid (center-of-mass) method (Morgan et al. 1989; Alexander and Ng 1991), the Gaussian interpolation (Willert and Gharib 1991), a sinc interpolation (Lourenco and Krothapalli 1995; Roesgen 2003) or a polynomial interpolation (Chen and Katz 2005), which reduce the “pixel locking” or “peak locking” effect (Prasad et al. 1992; Lourenco and Krothapalli 1995; Fincham and Spedding 1997; Westerweel 1998; Christensen 2004).
- Windowing functions, which become zero at the interrogation area boundaries (Gui et al. 2000; Liao and Cowen 2005), reducing the effect of particle image truncation at the edges of the image sub-spaces (interrogation areas) to be correlated (Nogueira et al. 2001).¹
- Direct correlation with a normalization, which so far has been realized in three ways: asymmetrically, with a small interrogation area from the first image correlated with a larger area in the second image (Huang et al. 1993a; Fincham and Spedding 1997; Huang et al. 1997; Rohály et al. 2002), symmetrically, with two interrogation areas of the same size (Nogueira et al. 1999; Nobach et al. 2004) or bi-directional, combining an asymmetric direct correlation as above and a second direct correlation with a small interrogation area from the second image correlated with a larger area in the first image (Nogueira et al. 2001), originally introduced as a “symmetric” method, but nonetheless using image sub-spaces of different sizes.

H. Nobach (✉) · E. Bodenschatz
Max Planck Institute for Dynamics and Self-Organization,
Bunsenstr. 10, Göttingen, Germany
e-mail: holger.nobach@nambis.de

¹ Note that such windowing introduces a new error to the displacement estimation (of the basic FFT method), since the shape of the particle images becomes asymmetric and the center of the intensity distribution moves towards the origin of the interrogation areas (Westerweel 1997).

- Iterative shift and deformation of the interrogation areas (Huang et al. 1993b; Lecordier 1997; Fincham and Delerce 2000; Scarano and Riethmuller 2000; Scarano 2002) or image deformation (Jambunathan et al. 1995; Tokumaru and Dimotakis 1995; Nogueira et al. 1999; Scarano 2004; Astarita 2008; Schrijer and Scarano 2008) with different image interpolation schemes as, e.g. the widely used, bi-linear interpolation, or more advanced higher-order methods (Lourenco and Krothapalli 1995; Fincham and Delerce 2000; Roesgen 2003; Astarita and Cardone 2005; Chen and Katz 2005; Astarita 2006) including the bi-cubic splines and the Whittaker interpolation (Whittaker 1929; Scarano and Riethmuller 2000), also known as sinc or cardinal interpolation, which have found wide acceptance.

Even if some of the methods given here have been developed primary to increase the achievable spatial resolution, they are all useful to improve the accuracy of displacement estimation. In this study, only the achievable accuracy is investigated.

With iterative window shift and deformation or image deformation techniques, an accuracy of the order of 0.01 pixel or better has been reported (Lecordier 1997; Astarita and Cardone 2005; Nobach et al. 2005) based on synthetic test images. In contrast, the application to real images from experiments shows less optimistic results, where the limit usually observed is about 0.1 pixel. Only under special conditions, like in two-dimensional flows with carefully aligned light sheets, can better accuracy be achieved (Lecordier and Trinité 2006).

As shown below, one reason for the different achievable accuracies in simulations and experiments may be the fact that in experiments, particles usually change their position within the light sheet (Fig. 1a). Therefore, the particles are illuminated differently in the two consecutive exposures. Additionally, the different illumination is individually different for each particle due to their different starting positions perpendicular to the light sheet plane. The result is an individual variation of particle intensities (further denoted as “intensity variations”), even in a homogeneous flow without any velocity gradient. Intensity variations can easily be seen in images from a variety of PIV applications, where some particles become brighter between the two exposures, whereas other particles, even if close by, become darker (Fig. 2). Simulations often assume that different particles can have different intensities, but not that the intensities can vary between subsequent exposures. This scenario can be realized in experiments only in two-dimensional flows with light sheets exactly aligned parallel to the flow field (Fig. 1b). Other sources of intensity variations could be an offset between the light sheet of the two illumination pulses or fluctuating scattering properties

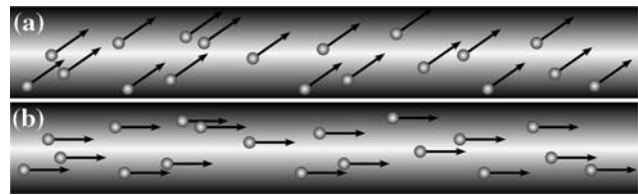


Fig. 1 Particles moving through a light sheet with an intensity profile: in **a** the particles have an out-of-plane velocity component and in **b** there is a two-dimensional flow aligned with the light sheet plane (only in-plane velocity components)

of the particles, e.g. non-spherical particles rotating in the flow.

Note that the effects of intensity variations are different from external large scale illumination variations (Huang et al. 1997), the intensity variations only due to the different particle locations within the light sheet without relative changes between the exposures (Westerweel 2000), or the loss-of-pairs and the degradation of the correlation peak due to out-of-plane motion (Keane and Adrian 1990, 1992; Keane et al. 1995; Westerweel 2000). While the loss-of-pairs and the degradation of the correlation peak increase the susceptibility to noise and the probability of outliers, the effect discussed here occurs additionally and directly affects the position of the correlation maximum.

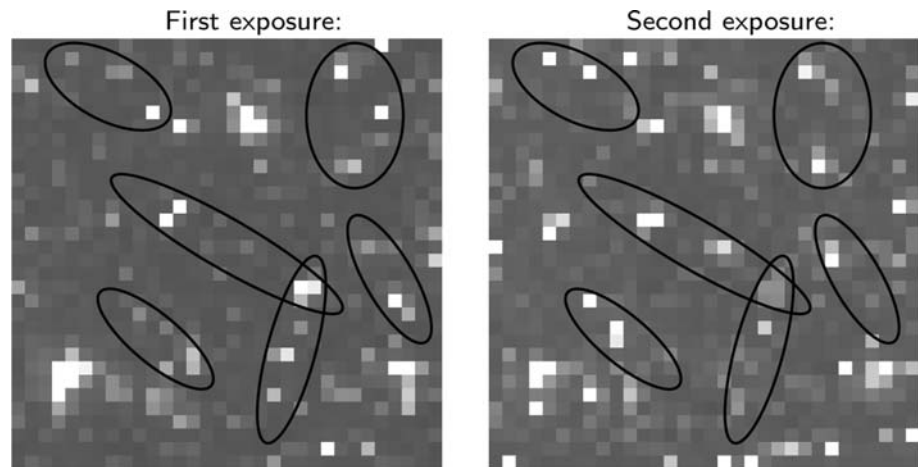
This paper shows the effect of intensity variations on the achievable accuracy of the correlation-based displacement estimation. The test procedures are simplistic to demonstrate the accuracy limiting effect of this phenomenon under otherwise ideal conditions. For more realistic images other effects may superimpose. An investigation of the pros and cons of the different PIV processing techniques, or a systematic comparison, are not topic of the present paper and are discussed elsewhere (see citations above).

The next section introduces the effect of intensity variations on the correlation-based PIV displacement estimation. Section 3 shows the particular results based on synthetic images, and Sect. 4 experimentally verifies the results. Finally, a discussion about the possibility to optimize the parameters of the PIV experiment to minimize the error is shown.

2 Effect of varying intensities

In PIV, the displacement of particle patterns between consecutive images is obtained from the peak position in the two-dimensional cross-correlation plane of the two images. Assuming (1) a certain number of imaged particles in the interrogation area, each with different intensity, but with the same relative intensity in the two consecutive images and (2) no truncation at the edges of the

Fig. 2 Examples demonstrating individual particle intensity variations (marked regions, detail of public PIV images from the PIV challenge 2003, case A, axisymmetric turbulent jet in stagnant surrounding, images A001a and A001b)



interrogation areas, the correlation peak is at the correct position, even if the particle images overlap and if the intensity of one entire image is scaled by a constant factor. Note the different meaning of “images”, which are the entire images to be correlated, and “particle images”, which are the spots at the particle positions. For demonstration, in Fig. 3 two images, each consisting of two well separated particle images (Airy discs), are correlated. The particles are at identical positions in the two images (no displacement between the images). The correct position of the correlation maximum at zero displacement can be seen clearly even for overlapping particle images and also with a constant scaling of one image (Fig. 3b).

This holds true also for the correlation of images with different relative amplitudes of the particle images, as long as the particle images do not overlap (Fig. 4a). With overlapping particle images and varying relative amplitudes (Fig. 4b), the maximum position of the correlation

peak is shifted, yielding a biased displacement estimate, depending on the amplitudes of the particle images, widths, and overlap.

The effect of an shifted correlation peak position for overlapping particle images can be seen also, if one of the two particle images is present in only one of the images, as it occurs if one particle moves out of the illumination plane. With a top-hat illumination profile, the amplitude of one of the particle images stays constant between the two exposures while the other particle image is absent in one of the two images. For well separated particle images (Fig. 5a) the correlation has its maximum at the correct position. As soon as the two particle images (in one of the two images) overlap, the correlation maximum is shifted (Fig. 5b).

The consequence for PIV image processing is an additional error in displacement estimates, if the intensities of particle images vary between the consecutive PIV images,

Fig. 3 Intensity and cross-correlation function (CC with lines of zero displacement in x and in y direction respectively and with the correlation maximum marked with a *black dot*) of two images (I and II), each consisting of two particle images: **a** same intensity of the particle images in the two images with well separated particle images and **b** one image scaled and with overlapping particle images

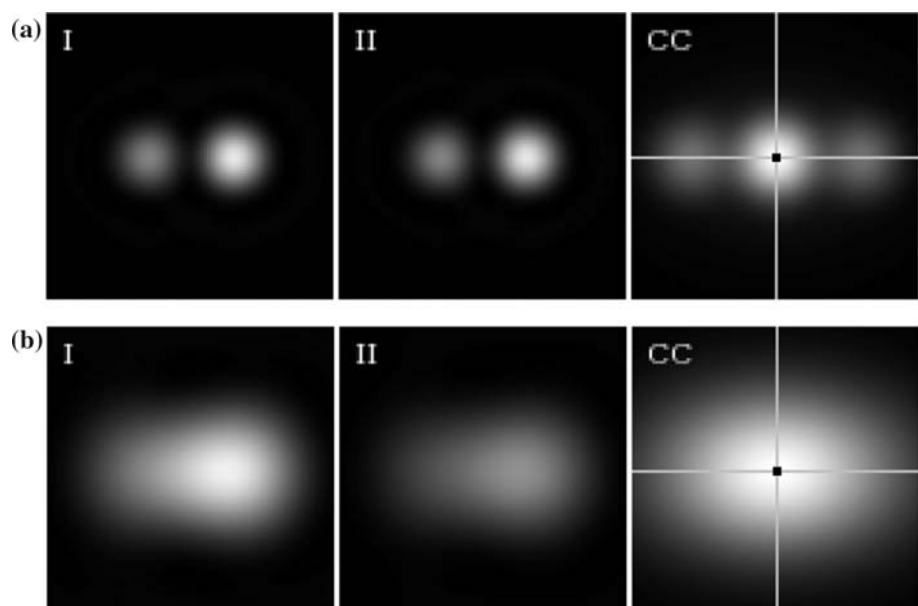


Fig. 4 Intensity and cross-correlation function (CC with lines of zero displacement in x and in y direction respectively and with the correlation maximum marked with a *black dot*) of two images (I and II), each consisting of two particle images: **a** varying relative intensity of well separated particle images and **b** varying relative intensity of overlapping particle images yielding a correlation peak with a shifted maximum location

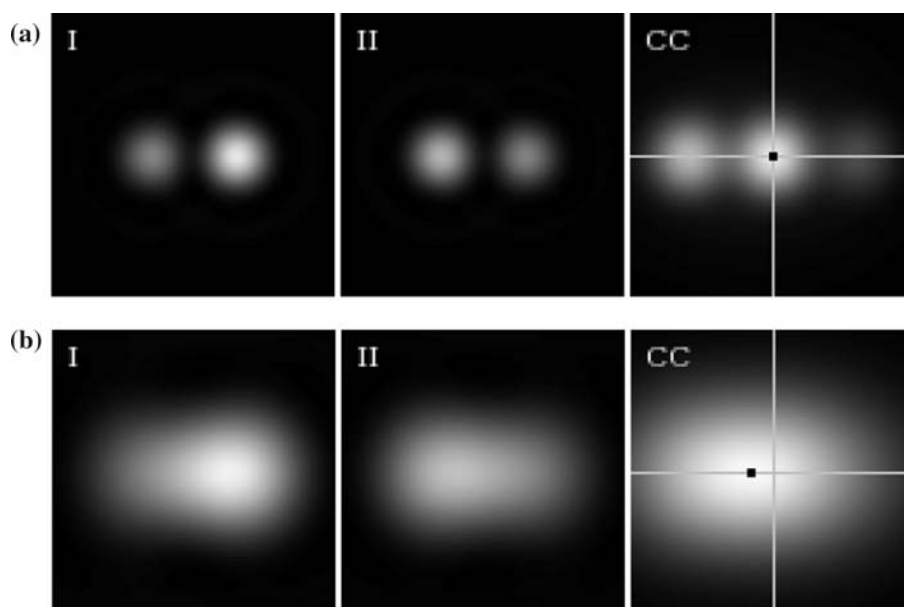
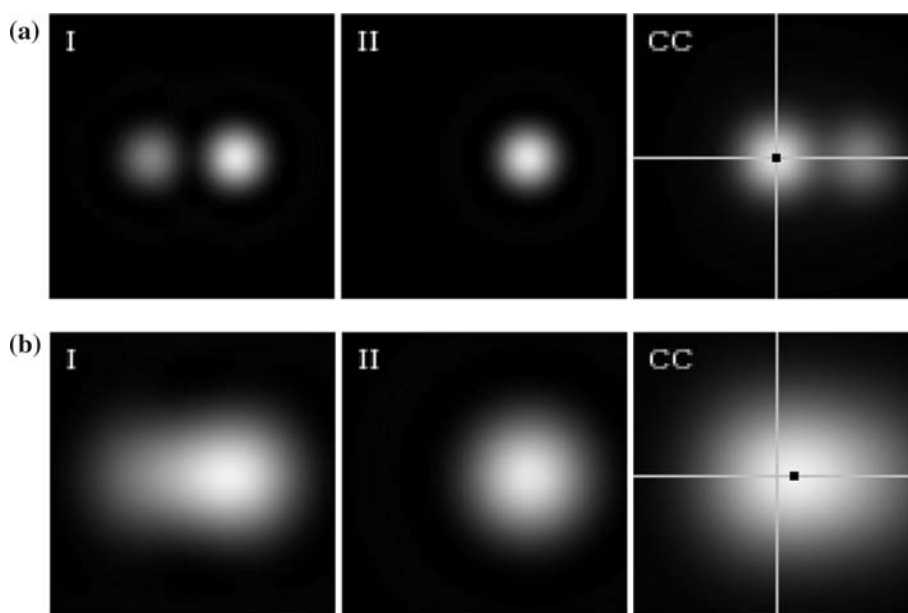


Fig. 5 Intensity and cross-correlation function (CC with lines of zero displacement in x and in y direction respectively and with the correlation maximum marked with a *black dot*) of two images (I and II), one consisting of two particle images and one with only one particle image (particle image drop-off): **a** drop-off with well separated particle images and **b** drop-off with overlapping particle images yielding a correlation peak with a shifted maximum location



while the particle images overlap. This error is especially large for de-focussed particle images (where the particle images tend to overlap) and in the case of misaligned light sheets or flows with out-of-plane motion of the particles (where the illumination of individual particles changes between the two light pulses). The influence of the particle number density will be shown to be negligible.

Note that for small particles with diffraction-limited imaging, only the intensity of a particle image depends on the particle position within the illumination profile, while the profile of the particle images is determined by the imaging system. Furthermore, note that the effect investigated here is not caused either by noise, or by the spatial

discretization of the particle images due to the pixel structure of the imaging system. These and other errors superimpose.

3 Test with synthetic images

The effect of intensity variations on the achievable accuracy of correlation-based PIV processing algorithms has been investigated using synthetic images.

The simulated particles are uniformly distributed within the light sheet and over the observation area. To consider the diffraction-limited imaging of small particles, the

simulated particle images are represented by Airy functions (diameter given by the first zero value), integrated over the sensitive sensor areas (pixels). The pixels are assumed to have a square shape with uniform sensitivity with a fill-factor of 1 (no gaps between the sensitive areas). The maximum intensities of the consecutive particle images are derived from the position perpendicular to the light sheet for each simulated particle, and individually for the two exposures. The light sheet is assumed to have either a Gaussian (the thickness is given by the e^{-2} value of the maximum intensity) or a top-hat profile. The Airy functions of overlapping particle images are linearly superimposed. To investigate the error of the displacement estimation, a series of 100 individual image pairs is generated (for each test case). The displacement of the particles between the two exposures is randomly chosen between -1 and $+1$ pixel simulating a variety of sub-pixel displacements. To isolate the effect of intensity variations from additional effects by, e.g. velocity gradients, the simulated displacement is constant for all particles, imitating a homogeneous velocity field.

To demonstrate the limitation in accuracy of correlation-based PIV algorithms due to intensity variations, an iterative window shift method with Whittaker interpolation, widely accepted as one of the best methods so far, is used exemplarily. Other PIV processing algorithms and interpolation schemes are affected differently. A systematic study can be found in Nobach and Bodenschatz (2007) and Sect. 5 gives characteristic model parameters of the error for commonly used PIV algorithms. However, in most cases, the differences according to this specific error are not significant. Other pros and cons of the algorithms are discussed elsewhere (see citations in the introduction).

The displacement estimator utilizes the peak position of the cross-correlation of the two images obtained by means of the fast Fourier transform (FFT). The sub-pixel location of the maximum is obtained by fitting a Gaussian function to the maximum of the correlation and its two direct neighbors in x and y direction separately. In the next and all following iteration steps, the two consecutive images are interpolated using the Whittaker interpolation (Whittaker 1929; Scarano and Riethmuller 2000), realized here with an 8×8 pixels kernel, and re-sampled at positions shifted symmetrically by plus/minus half the pre-estimated displacement. For a correct displacement estimate of the original images, the two re-sampled images are identical and no displacement can be found between them. Remaining displacements are used to iteratively correct the displacement pre-estimate. This iterative correction loop asymptotically approaches a vanishing displacement between the two re-sampled interrogation areas. To keep the investigations simple and to isolate the influence of intensity variations, window deformation has not been

implemented here to avoid other well-known effects, such as limited spatial resolution or dynamic range issues, which may additionally influence the results. However, the conclusions are equally applicable to the case of velocity fields with gradients. In that case the other error sources sum.

The difference between the simulated and the displacement estimated by the above procedure gives an individual estimation error. From the series of individual errors, an averaged RMS error is derived. To separate the RMS error due to the limited accuracy and the dominating influence of outliers a simple outlier detection algorithm has been implemented. All displacement estimates outside a range of ± 1 pixel around the expected value are assumed to be outliers and are not taken into account for the calculation of the RMS error. From the number of outliers the probability of outliers is estimated. More reliable outlier detection algorithms based on statistical properties of the surrounding vector field as, e.g. in Westerweel and Scarano (2005) could not be used in this simulation because it includes only single displacement vectors.

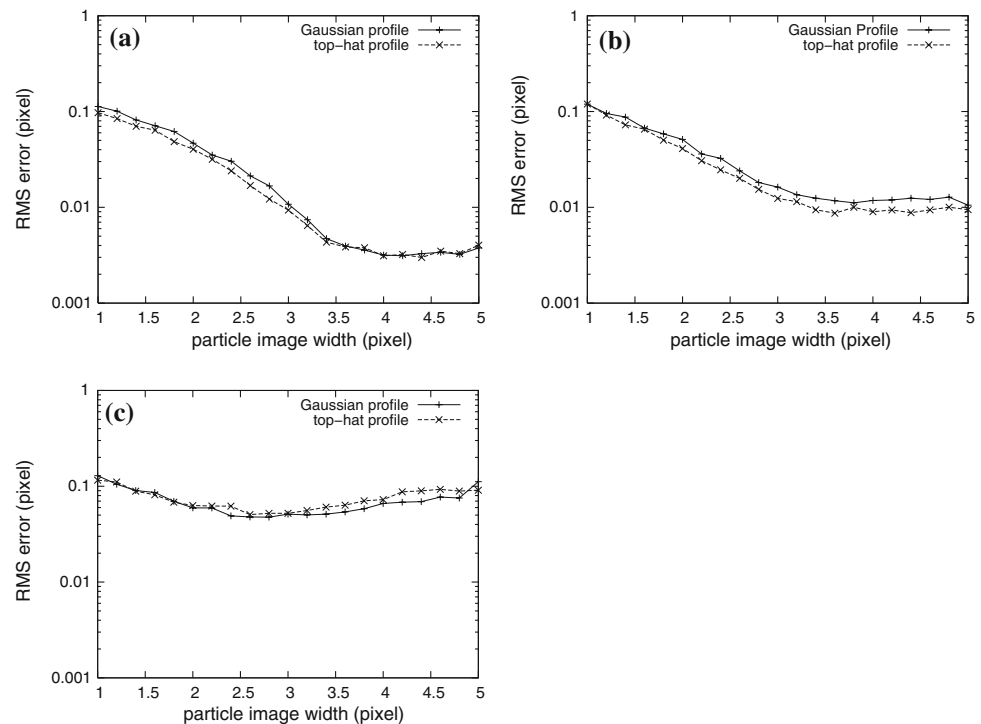
In the first test case, the RMS error of the algorithm given above is investigated as a function of the particle image diameter. The particle number density is 20 in an interrogation area of 32×32 pixels.

In Fig. 6a the results are shown for only in-plane motion (without noise). The RMS deviation clearly drops below 0.01 pixel for particle image diameters larger than 3 pixels. For smaller particle images the effect of under-sampling occurs and limits the achievable estimation accuracy to about 0.1 pixel for a particle image diameter of 1 pixel. The differences between the two light sheet profiles are not significant.

The simulation of only in-plane motion has also been done with photon noise (1,000 photo electrons giving about 32 electrons noise, 10 electrons per count then give an corresponding image intensity of 100) and quantization noise (only integer counts). No background gray values have been added. The RMS deviation in the range above 3 pixels is significantly higher than in the previous simulation limiting the achievable accuracy to about 0.01 pixel (Fig. 6b). The range below 3 pixel particle image diameters is dominated by under-sampling.

An out-of-plane component of the displacement has a much stronger influence than the noise. Between the two exposures, the individual particles change their position in a direction perpendicular to the light sheet. Depending on its starting position, the illumination of a particle changes individually, even if the in-plane and the out-of-plane displacements are the same for all particles. In Fig. 6c the effect of an out-of plane displacement of $1/4$ of the light sheet thickness is shown. The out-of-plane motion, even without noise, limits the achievable accuracy to about 0.05 pixel when the particle image diameter is at its optimum of about 3 pixels.

Fig. 6 RMS deviation of the displacement estimate as a function of the particle image diameter for **a** in-plane motion only (without noise), **b** in-plane motion with simulated noise and **c** motion with an out-of-plane component ($1/4$ of the light sheet thickness, without noise)



To show how important the out-of-plane displacement is, the simulation has been done also with the optimum particle image diameter, which we found is 3 pixels, but with varying out-of-plane displacement, interrogation area size and particle number density (Fig. 7). All other simulation and estimation parameters remain unchanged from the simulation above.

The out-of-plane displacement has the strongest influence (Fig. 7a). The RMS error increases exponentially starting at about 0.01 pixel for only in-plane motion, and 0.1 pixel for an out-of-plane displacement of $1/2$ the light sheet thickness. The RMS error approaches about 1 pixel at an out-of-plane displacement of one full light sheet thickness. The difference between the two light sheet profiles is small but significant. Generally, the RMS error is more strongly influenced by the out-of-plane component with a Gaussian profile than with a top-hat profile. However, the RMS error with a top-hat profile tends to be larger than that for a Gaussian profile in the preferable range of small out-of-plane displacements. The probability of outliers increases with the out-of-plane displacement, limiting the useful range to a maximum out-of-plane displacement of about $1/2$ of the light sheet thickness for a Gaussian light sheet profile, where outliers are rare. Note that this value holds only when particles all have the same scattering characteristics. Populations of particles with varying scattering characteristics (e.g. particles of different sizes) shift the maximum acceptable out-of-plane displacement toward smaller values. The onset of high probability of outliers is

shifted towards larger out-of-plane displacements for the top-hat profile. However, it is wrong to conclude that the top-hat profile is superior compared to the Gaussian profile, since the integral of the intensity profile for the Gaussian profile yields a total intensity of only 63% compared to a top-hat profile of the same width (using the common definition of the light sheet thickness with Gaussian shape based on the e^{-2} values of the maximum intensity). Alternative definitions of the light sheet thickness stretch the argument of relative out-of-plane displacement in Fig. 7a arbitrarily and hence, may change the slope of RMS error and shift the outlier probability.

The estimation accuracy can be improved by increasing the size of the interrogation areas, because the displacement errors average (Fig. 7b). For a constant particle number density, the RMS value decreases as the inverse of the linear dimension of the interrogation area, giving slightly more than 0.1 pixel for an interrogation area of 12×12 pixels and slightly more than 0.01 pixel at 128×128 pixels. For too small an interrogation area, outliers occur as expected, because too few particles are present in the interrogation area, which leads to mismatched particles in the two exposures.

In contrast to the two previous influences, varying the particle number density (Fig. 7c) has almost no effect on the RMS error. Here, the increased information due to the increased number of particle images in the interrogation area and the increased probability of overlapping particle images with the resulting influence of the intensity

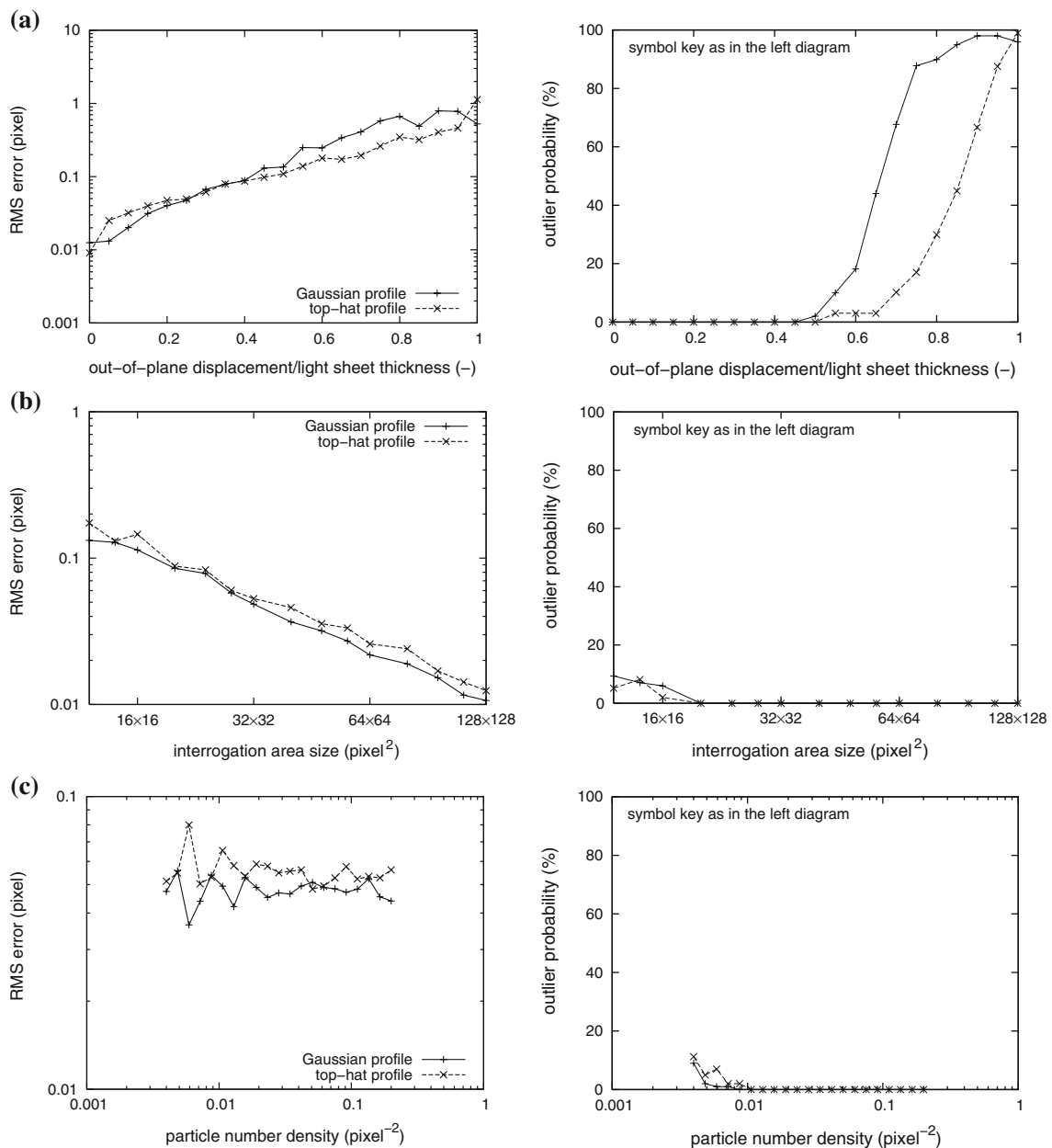


Fig. 7 RMS deviation and outlier probability of the displacement estimate **a** as a function of the out-of-plane displacement component; **b** as a function of the interrogation area size; **c** as a function of the particle number density (standard values if not changed: particle

image diameter: 3 pixels, particle number density: $0.0195 \text{ pixel}^{-2}$, interrogation area: 32×32 pixels, out-of-plane motion: $1/4$ of the light sheet thickness, without noise)

variations compensate for each other. For a particle number density below 0.01 pixel^{-2} the estimate becomes unreliable and yields outliers. This is for an interrogation area of 32×32 pixels, yielding about 10 particles per interrogation area. The value of the minimum particle number density depends on the chosen interrogation area size (Raffel et al. 1998).

One might question the result that the particle number density is negligible. In order to address this, in Fig. 8 the

RMS errors for two more out-of-plane displacements are shown (0 and $1/8$ of the light sheet thickness). Without out-of-plane displacements, the number of successfully correlated particle images increases linearly with the particle number density. For each particle, the correlation of the images has a small stochastic error, caused e.g. by intensity interpolation over the pixel areas or by errors during image interpolation. The individual errors average over all particles in the interrogation area, yielding an RMS error

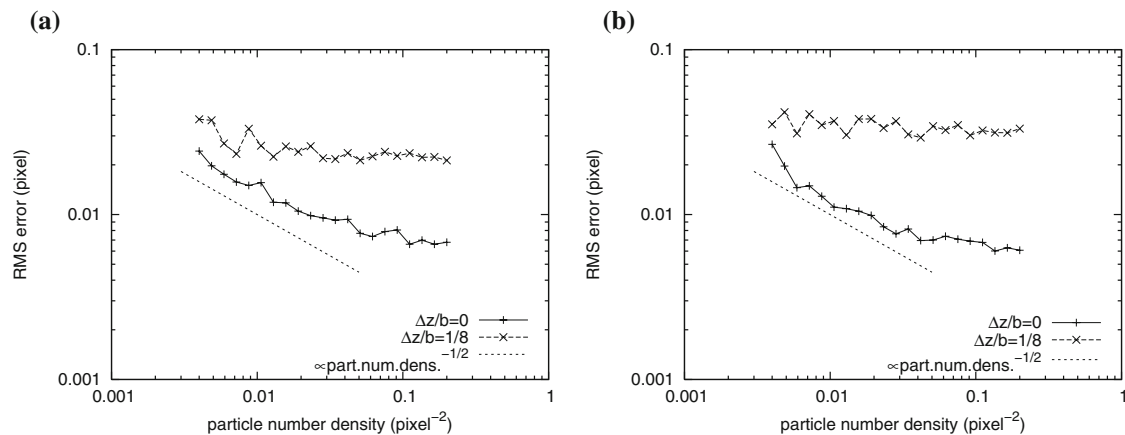


Fig. 8 RMS deviation of the displacement estimate as a function of the particle number density; parameters as in Fig. 7, except for the out-of-plane displacement Δz normalized with the light sheet

decreasing with the square root of the particle number density. This complies with Westerweel (2000) (there for low particle densities) and it can be seen in Fig. 8 for both, the Gaussian and the top-hat profile, for particle number densities up to about 0.05 pixel^{-2} . Beyond this value a lower boundary of the RMS error occurs, caused by remaining interpolation errors of the correlation function. This error does not decrease with further increased particle number density. Note, that the particle density at this transition point is much lower than that at the transition from individual particle images to a homogeneous speckle pattern.

If there is a certain out-of-plane displacement, the previous errors are superimposed by the strong influence of intensity variations of overlapping particle images. In contrast to the number of successfully correlated particle images, the probability of overlapping particle images increases with the square of the particle number density. Each of these pairs of overlapping particle images contributes a stochastic error to the correlation. After averaging the individual errors of overlapping pairs of particle images over the number of particles in the interrogation area, these two contributions exactly compensate, and the observed error becomes independent of the particle number density.

4 Experimental verification

Experimental verification of the results given above requires a PIV setup with an adjustable beam shape (and width) and an adjustable out-of-plane component of the real velocity field. The first requirement can be realized with a video projector imaging different intensity profiles into the measurement volume using an additional collimation lens (Fig. 9). To achieve stable illumination, LCD

thickness b ($\Delta z/b = 0$ and $1/8$) for **a** a Gaussian light sheet profile and for **b** a top-hat profile (without noise)

technology is preferred. The projector with DLP technology used here realizes individual gray values by pulse width modulation, which causes illumination problems with PIV cameras at short exposure (integration) times. In the present study the exposure time has been set to 0.25 s, which corresponds to 30 illumination cycles of the DLP chip, since it works at a frame rate of 120 Hz. This long exposure time requires small velocities, which have been realized by moving a solid glass block on a three-dimensional translation stage. The glass block has a size of $5 \text{ cm} \times 5 \text{ cm} \times 8 \text{ cm}$ and includes 54,000 randomly distributed dots in the inner $3 \text{ cm} \times 3 \text{ cm} \times 6 \text{ cm}$ volume, corresponding to a particle density of 1 mm^{-3} .

Verification of the results requires an accurate synchronization of the in-plane and the out-of-plane translation through the light sheet. To avoid problems, the system has been inverted. The glass block moves along one axis of the translation stage, and the plane of illumination is tilted with respect to the axis of motion. While the glass block is translated with a constant velocity of 0.1 mm s^{-1} through the observation area of the camera, a series of 80 images with 480×480 pixels size is taken at a frame rate of 0.8 Hz. By choosing the number of frames between the two frames to be correlated, different out-of-plane components can be imitated. For better statistics, 9×11 displacement vectors have been calculated for each pair of images with non-overlapping interrogation areas. Furthermore, the results for all image pairs with the same number of frames between them, selected from the original series of 80 images, have been averaged.

Three different cases have been investigated for both, a Gaussian and a top-hat profile type (Table 1). The first case is without an out-of-plane component, the light sheet is aligned with the translation of the glass block. In the second case the light sheet is tilted by an x -to- y ratio of 0.75. Depending on the light sheet type, the out-of-plane

Fig. 9 Sketch of the experimental setup: a video projector is imaging different illumination profiles into the measurement volume, which is observed by a digital camera. A glass block with internal markers is translated vertically through the measurement volume

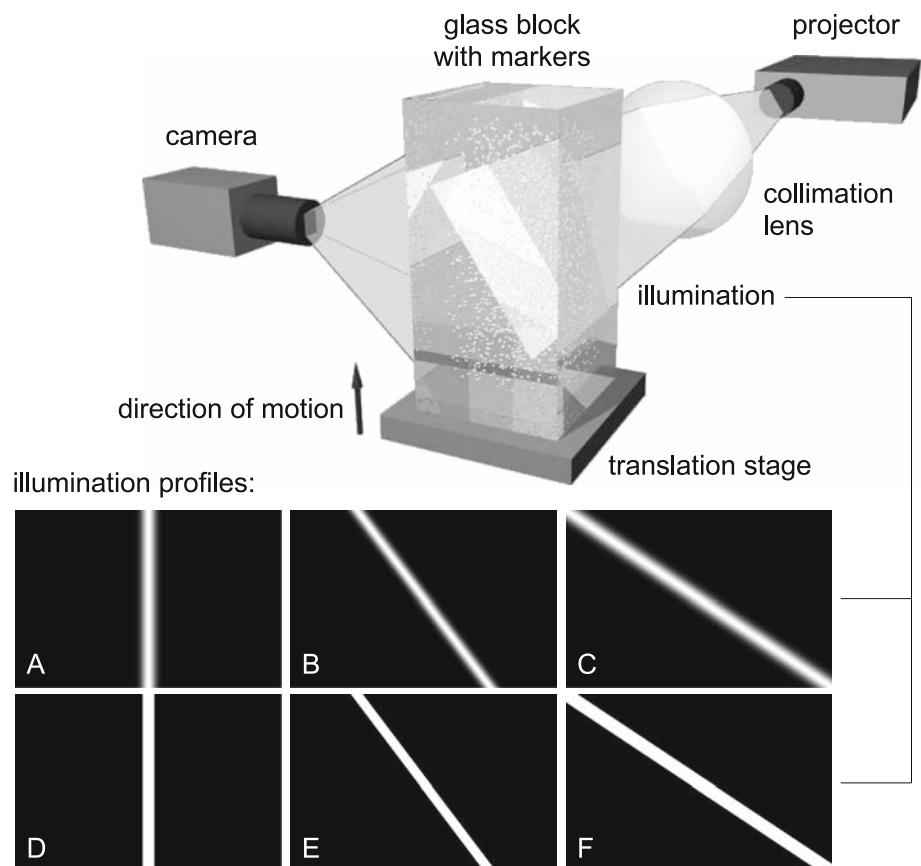


Table 1 Light sheet characteristics for the experimental verification

Case	Profile type	Width (mm)	Slope	Out-of-plane component
A	Gaussian	3.1 ^a	0	0
B	Gaussian	3.1 ^a	0.75	1/(33.3 frames)
C	Gaussian	6.3 ^a	1.5	1/(33.3 frames)
D	Top-hat	2	0	0
E	Top-hat	2	0.75	1/(21.2 frames)
F	Top-hat	4	1.5	1/(21.2 frames)

^aDefined by the e^{-2} of the maximum amplitude

displacement speed is one light sheet thickness after 41.7 s for the Gaussian profile and 26.7 s for the top-hat profile, corresponding to a total of 33.3 and 21.2 frames, respectively, in the series of PIV images. In the third case both the light sheet width and the slope are doubled. This produces a doubled particle image density, while the out-of-plane velocity component, after normalization with the light sheet thickness, remains constant.

Figure 10a and b shows the results for the Gaussian and the top-hat profile types, respectively. Without an out-of-plane component, the accuracy of the displacement estimation does not depend on the frame distance (profiles A

and D). Because the difference between the correlated images is a simple translation, the accuracy of about 0.05 pixel corresponds to a mixture of the mechanical accuracy of the translation stage and the sub-pixel resolution of the PIV processing method.

Using the tilted profiles B, C, E and F, the illumination of the particles changes depending on the frame distance, imitating different out-of-plane components. Corresponding to Fig. 7a, the RMS error increases with the frame distance. Since profiles C and F have doubled width and slope compared to profiles B and E, the imitated out-of-plane displacement normalized with the light sheet thickness is the same, while the particle image density is doubled. Corresponding to Fig. 7c, the coincidence of the RMS error for different particle image densities shows that the particle image density plays a minor role. Again, the difference between the two light sheet profile types is small but significant. The influence of the out-of-plane component is stronger and the slope of the curve is steeper for the Gaussian profile than for the top-hat profile.

For a direct comparison of the experimental data and the simulation, a new simulation has been made adapting the experimental parameters, which are particle image diameter 3.0 pixel, interrogation areas 32×32 pixels, iterative

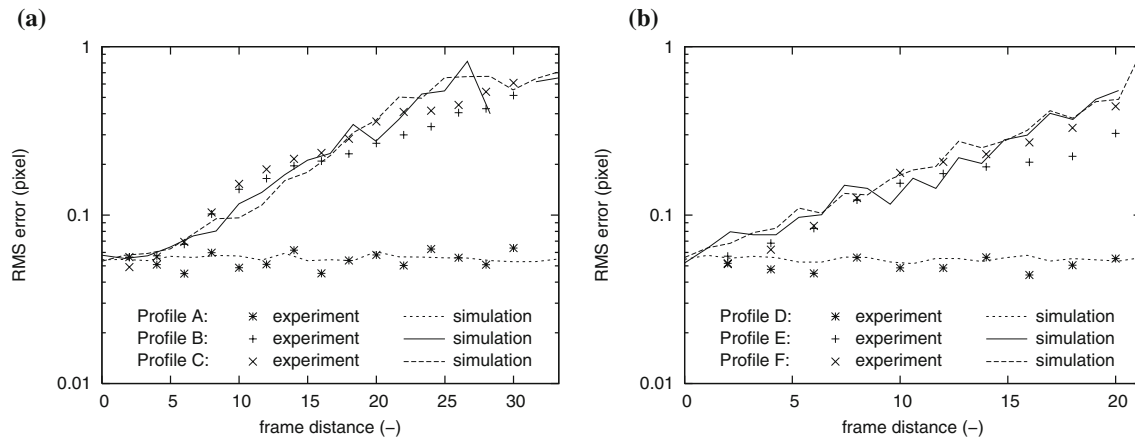


Fig. 10 Experimentally obtained RMS variation of the displacement estimate using the iterative interrogation area shift with bi-linear image interpolation as a function of the frame distance in comparison to the simulation for **a** a Gaussian light sheet profile and for

b a top-hat profile (abscissas' limits directly correspond to an out-of-frame displacements between zero and one light sheet thickness for profiles B, C, E and F)

interrogation area displacement without deformation, bi-linear image interpolation, outlier detection level of ± 1 pixel in x and y direction, particle densities: 10.33 (profiles A and B), 20.66 (profile C), 6.57 (profiles D and E) and 13.14 (profile F) particles within the interrogation area. An important difference with the previous simulation is that only one-dimensional displacement is simulated, as is the case for the experiment. The displacement estimation, however, is two-dimensional in all cases. The results in Fig. 10 show good agreement between experiment and simulation, verifying both the effect of the intensity variations and the simulation procedure.

5 Discussion and optimization

To minimize the effect of intensity variations, the out-of-plane component should be small compared to the width of the light sheet. For a given flow with a certain out-of-plane velocity the normalized out-of-plane component can be minimized by increasing the light sheet thickness or decreasing the time between the two exposures. Unfortunately, this deteriorates the spatial resolution or the accuracy of the in-plane velocity estimate. In practice, to optimize the experimental parameters, these errors should be balanced.

From Fig. 7a and b the RMS error of the displacement estimation can be found to be of the type

$$\sigma_{\Delta x} = c_0 c_1 a^{c_2} e^{c_3 \Delta z / b} \quad (1)$$

with the linear dimension of the interrogation area a , the out-of-plane displacement Δz and the light sheet thickness b . The calibration constant c_0 transforms the image coordinates

(in pixels) into real world coordinates (in meters). The values of the model parameters c_1 , c_2 and c_3 depend on the PIV processing method. In Table 2, parameters are given for commonly used methods found from simulations, as above, for a simulated particle image diameter of 3 pixels. The model parameters are derived by a fit to samples taken at out-of-plane displacements of 1/4, 1/2 and 3/4 of the light sheet thickness, and interrogation area sizes of 32×32 , 64×64 and 128×128 pixels.

The out-of-plane displacement Δz is

$$\Delta z = w \Delta t \quad (2)$$

with the out-of-plane velocity w and the time Δt between the two exposures. The in-plane velocity u is derived from the displacement Δx as

$$u = \frac{\Delta x}{\Delta t}$$

yielding the RMS error of the velocity estimation

$$\sigma_u = \frac{1}{\Delta t} c_0 c_1 a^{c_2} e^{c_3 w \Delta t / b} \quad (4)$$

which is a convex function with a minimum at $\Delta t = b / (c_3 w)$. Since c_3 varies between 4.0 and 4.5 for the Gaussian light sheet profile and between 2.5 and 2.8 for the top-hat light sheet profile (except for the bi-linear interpolation with smaller c_3 but with generally quite large RMS errors and the Whittaker interpolation with a larger c_3 but with generally quite small RMS errors; Table 2) the optimum Δt is reached with a particle out-of plane motion of 2/9 to 2/5 of the light sheet thickness between the exposures, depending on the processing algorithm and the light sheet profile, which roughly complies with intuition and common practice (Raffel et al. 1998).

Table 2 Error model parameters (particle image diameter: 3 pixels; particle number density: 0.0195 pixel⁻²)

PIV method	Gaussian profile			Top-hat profile		
	c_1	c_2	c_3	c_1	c_2	c_3
FFT with ...						
... no (rectangular) window	0.50	-0.89	4.0	0.80	-0.90	2.5
... polynomial window ^a	0.65	-0.86	4.0	1.20	-0.92	2.7
... cosine to the 20th window ^b	0.40	-0.86	4.3	0.71	-0.88	2.6
... Gaussian window ^c	0.45	-0.83	4.3	1.08	-0.90	2.6
direct correlation with ...						
... asymmetrical normalization ^d	0.43	-0.88	4.1	0.70	-0.88	2.6
... asymmetrical, bi-directional normalization ^e	0.40	-0.87	4.2	0.66	-0.87	2.6
... symmetrical normalization ^f	0.38	-0.86	4.1	0.61	-0.85	2.6
interrogation window shift with ...						
... bi-linear image interpolation	0.31	-0.49	2.7	0.58	-0.55	1.5
... Whittaker image interpolation ^g	0.45	-1.00	4.8	1.12	-1.09	3.1
... bi-cubic spline image interpolation	0.34	-0.80	4.1	0.75	-0.87	2.5
... Gaussian low-pass image interpolation ^h	1.40	-0.99	4.5	2.33	-0.98	2.8

^aNogueira et al. (1999); ^bLiao and Cowen (2005); ^cGui et al. (2000); ^dHuang et al. (1993a), Fincham and Spedding (1997), Huang et al. (1997), Rohály et al. (2002); ^eNogueira et al. (2001); ^fNogueira et al. (1999), Nobach et al. (2004); ^gWhittaker (1929), Scarano and Riethmuller (2000); ^hNobach et al. (2005)

6 Conclusion

The effect on the obtainable accuracy of a PIV system of particle image intensities varying individually between the two consecutive images has been investigated. Such intensity variations occur in experiments due to the motion of the particles in the intensity profile of the light sheet, misalignments of the two light pulses or changes of the particle's scattering properties between the two exposures. This effect limits the obtainable accuracy of PIV measurements, even under otherwise ideal conditions. The commonly used best practice parameters for PIV experiments could be verified (particle image diameter of 3 pixels) or specified (out-of-plane displacement of 2/9 through 2/5 of the light sheet thickness depending on the method of PIV analysis). The usually observed accuracy limit of the order of 0.1 pixel could be shown. This value is almost independent of the particle number density, but it strongly increases with increasing out-of-plane displacements, and decreases with increasing interrogation area size.

The error has been quantified for several commonly used PIV processing methods. The iterative window shift method with bi-cubic spline or Whittaker image interpolation performs best. The widely used bi-linear interpolation is worse than the simple FFT method. The Gaussian low-pass filter image interpolation (Nobach et al. 2005), which performs excellently without the intensity variations, has the highest RMS error of all methods when intensity variations are present.

In summary, besides under-sampling, the variations of the particle image intensities are an additional error, dominating the range of particle image diameters of larger than 3 pixels. This error leads to a basic limitation of the PIV technique and could explain the accuracy limit of PIV of about 0.1 pixel usually seen in experiments.

Acknowledgments The authors appreciate the kind help of Gregory Bewley.

Open Access This article is distributed under the terms of the Creative Commons Attribution Noncommercial License which permits any noncommercial use, distribution, and reproduction in any medium, provided the original author(s) and source are credited.

References

- Alexander BF, Ng KC (1991) Elimination of systematic error in sub-pixel accuracy centroid estimation. *Opt Eng* 30:1320–1331
- Astarita T (2006) Analysis of interpolation schemes for image deformation methods in PIV: effect of noise on the accuracy and spatial resolution. *Exp Fluids* 40:977–987
- Astarita T (2008) Analysis of velocity interpolation schemes for image deformation methods in PIV. *Exp Fluids* 45:257–266
- Astarita T, Cardone G (2005) Analysis of interpolation schemes for image deformation methods in PIV. *Exp Fluids* 38:233–243
- Chen J, Katz J (2005) Elimination of peak-locking error in PIV analysis using the correlation mapping method. *Meas Sci Technol* 16:1605–1618
- Christensen KT (2004) The influence of peak-locking errors on turbulence statistics computed from PIV ensembles. *Exp Fluids* 36:484–497
- Fincham A, Delerce G (2000) Advanced optimization of correlation imaging velocimetry algorithms. *Exp Fluids* 29:S13–S22

- Fincham AM, Spedding GR (1997) Low cost, high resolution DPIV for measurement of turbulent fluid flow. *Exp Fluids* 23:449–462
- Gui L, Merzkirch W, Fei R (2000) A digital mask technique for reducing the bias error of the correlation-based PIV interrogation algorithm. *Exp Fluids* 29:30–35
- Huang HT, Fiedler HE, Wang JJ (1993a) Limitation and improvement of PIV; Part I: Limitation of conventional techniques due to deformation of particle image patterns. *Exp Fluids* 15:168–174
- Huang HT, Fiedler HE, Wang JJ (1993b) Limitation and improvement of PIV; Part II: Particle image distortion, a novel technique. *Exp Fluids* 15:263–273
- Huang H, Dabiri D, Gharib M (1997) On errors of digital particle image velocimetry. *Meas Sci Technol* 8:1427–1440
- Jambunathan K, Ju XY, Dobbins BN, Ashforth-Frost S (1995) An improved cross correlation technique for particle image velocimetry. *Meas Sci Technol* 6:507–514
- Keane RD, Adrian RJ (1990) Optimization of particle image velocimeters. Part I: Double pulsed systems. *Meas Sci Technol* 1:1202–1215
- Keane RD, Adrian RJ (1992) Theory of cross-correlation analysis of PIV images. *Appl Sci Res* 49:191–215
- Keane RD, Adrian RJ, Zhang Y (1995) Super-resolution particle imaging velocimetry. *Meas Sci Technol* 6:754–768
- Lecordier B (1997) Etude de l'interaction de la propagation d'une flamme prémélangée avec le champ aérodynamique, par association de la tomographie laser et de la vélocimétrie par images de particules. Ph.D. thesis, l'Université de Rouen, France
- Lecordier B, Trinité M (2006) Accuracy assessment of image interpolation schemes for PIV from real images of particle. In: Proceedings of 13th international symposium on applications of laser techniques to fluid mechanics, Lisbon, Portugal, paper 26.4
- Liao Q, Cowen EA (2005) An efficient anti-aliasing spectral continuous window shifting technique for PIV. *Exp Fluids* 38:197–208
- Lourenco L, Krothapalli A (1995) On the accuracy of velocity and vorticity measurements with PIV. *Exp Fluids* 18:421–428
- Morgan JS, Slater DC, Timothy JG, Jenkins EB (1989) Centroid position measurements and subpixel sensitivity variations with the MAMA detector. *Appl Opt* 28(6):1178–1192
- Nobach H, Bodenschatz E (2007) Limitations of accuracy in PIV due to individual variations of particle image intensities. In: Proceedings of 7th international symposium on particle image velocimetry, Rome, Italy
- Nobach H, Damaschke N, Tropea C (2004) High-precision sub-pixel interpolation in PIV/PTV image processing. In: Proceedings of 12th international symposium on applications of laser techniques to fluid mechanics, Lisbon, Portugal, paper 24.1
- Nobach H, Damaschke N, Tropea C (2005) High-precision sub-pixel interpolation in particle image velocimetry image processing. *Exp Fluids* 39:299–304
- Nogueira J, Lecuona A, Rodríguez PA (1999) Local field correction PIV: on the increase of accuracy of digital PIV systems. *Exp Fluids* 27:107–116
- Nogueira J, Lecuona A, Rodríguez PA (2001) Identification of a new source of peak locking, analysis and its removal in conventional and super-resolution PIV techniques. *Exp Fluids* 30:309–316
- Prasad AK, Adrian RJ, Landreth CC, Offutt PW (1992) Effect of resolution on the speed and accuracy of particle image velocimetry interrogation. *Exp Fluids* 13:105–116
- Raffel M, Willert C, Kompenhans J (1998) Particle image velocimetry: a practical guide. Springer, Berlin
- Roesgen T (2003) Optimal subpixel interpolation in particle image velocimetry. *Exp Fluids* 35:252–256
- Rohály J, Frigerio F, Hart DP (2002) Reverse hierarchical PIV processing. *Meas Sci Technol* 13:984–996
- Scarano F (2002) Iterative image deformation methods in PIV. *Meas Sci Technol* 13:R1–R19
- Scarano F (2004) On the stability of iterative PIV image interrogation methods. In: Proceedings of 12th international symposium on applications of laser techniques to fluid mechanics, Lisbon, Portugal, paper 27.2
- Scarano F, Riethmuller ML (2000) Advances in iterative multigrid PIV image processing. *Exp Fluids* 29:S51–S60
- Schrijer FFJ, Scarano F (2008) Effect of predictor–corrector filtering on the stability and spatial resolution of iterative PIV interrogation. *Exp Fluids* 45:927–941
- Tokumaru PT, Dimotakis PE (1995) Image correlation velocimetry. *Exp Fluids* 19:1–15
- Utami T, Blackwelder RF, Ueno T (1991) A cross-correlation technique for velocity field extraction from particulate visualization. *Exp Fluids* 10:213–223
- Westerweel J (1993) Digital particle image velocimetry: theory and application. Delft University Press, Delft, The Netherlands
- Westerweel J (1997) Fundamentals of digital particle image velocimetry. *Meas Sci Technol* 8:1379–1392
- Westerweel J (1998) Effect of sensor geometry on the performance of PIV interrogation. In: Proceedings of 9th international symposium on applications of laser techniques to fluid mechanics, Lisbon, Portugal, paper 1.2
- Westerweel J (2000) Theoretical analysis of the measurement precision in particle image velocimetry. *Exp Fluids* 29:S3–S12
- Westerweel J, Scarano F (2005) Universal outlier detection for PIV data. *Exp Fluids* 39:1096–1100
- Whittaker JM (1929) The Fourier theory of the cardinal functions. *Proc R Soc Edinb Sect A Math* 1:169–176
- Willert CE, Gharib M (1991) Digital particle image velocimetry. *Exp Fluids* 10:181–193